GEOLOGICAL SURVEY OF CANADA

OPEN FILE 2296

Preliminary report of data acquisition and processing for the 1989-1990 Lincoln Sea Aeromagnetic Survey

B. Nelson, D. Hardwick, D.A. Forsyth,
D. Marcotte, D. Teskey, M. MacPherson,
M. Bower, R. Macnab

1991

Final Copy, GSC Open File 2296 November 21, 1990

PRELIMINARY REPORT OF DATA ACQUISITION AND PROCESSING FOR THE 1989-1990 LINCOLN SEA AEROMAGNETIC SURVEY

B. Nelson[1], D. Hardwick[2], D.A. Forsyth[3], D. Marcotte[2], D. Teskey[4], M. MacPherson[1], M. Bower[2], R. Macnab[5],

1. Defence Research Establishment Pacific, Victoria BC
2. Institute for Aerospace Research, Ottawa ONT
3. Continental Geoscience Division, Ottawa ONT
4. Geophysics Division, Ottawa ONT
5. Atlantic Geoscience Centre, Dartmouth NS

ABSTRACT

The aeromagnetic survey of the Lincoln Sea, which was initiated in 1989 and continued in 1990, is expected to be completed in 1991. The work is the result of a coordinated effort by the Department of National Defence, the Geological Survey of Canada, and the Canadian Institute for Aerospace Research. With a line spacing of 4 km, this is the most detailed aeromagnetic survey in the Arctic north of 82°N. In addition, it is the first aeromagnetic survey which extends over northern Ellesmere Island and Greenland. This open file describes the extensive operational systems, the survey parameters and the results of a preliminary analysis of the 1989 and 1990 data. Anomalies are associated with geological terranes such as the Northern Ellesmere Magmatic Belt, the Robeson Channel between Ellesmere Island and Greenland, possible intrusive sources, and the transition from continental to oceanic crust.

Depth-to-source estimates have been made from the raw profile data assuming two-dimensional structures perpendicular to the flight path. These estimates suggest that there are three main types of magnetic source in the southern Lincoln Sea: relatively strong magnetic sources, such as mafic intrusions, within about 500 m of the sea-floor; a magnetic basement which lies several km beneath the sea-floor; and shallow sources (less than 700 m) which are either not very magnetic, or are physically small.

1. INTRODUCTION

The aeromagnetic survey of the Lincoln Sea, which was initiated in 1989 and continued in 1990, is expected to be completed in 1991. Funding was provided by the Department of National Defence (DND), the Geological Survey of Canada (GSC), and the Institute for Aerospace Research (IAR). The Convair 580 aircraft operated by IAR was used to collect the data. A total of approximately 20,000 line-km has already been flown, and a further 2,500 line-km is planned for 1991.

Existing aeromagnetic data (Forsyth et al, 1990) in this area have a line spacing of approximately 20 km. The new surveys represent the first relatively detailed surveys this far north with spacings of 3-4 km and tie line spacings of approximately 50 km. In addition, these are the first aeromagnetic surveys which include significant data from northern Ellesmere Island and northern Greenland.

The tectonic history of the Lincoln Sea area is poorly constrained. From the north, the area contains possible effects resulting from the development of the Alpha Ridge, the Lomonosov Ridge, and the opening of the Fram Basin. From the south, clues to the nature of tectonic adjustments between Ellesmere Island and Greenland, including the area of Nares Strait, may be contained in the upper crust and represented in the magnetic anomaly pattern. The aim of these surveys is to provide meaningful constraints on crustal features related to the opening of this part of the Arctic Ocean.

This open file describes the survey parameters and outlines the results of a preliminary analysis of the 1989 and 1990 surveys.

2. REGIONAL GEOLOGY

Recent summaries of the regional geological and tectonic framework may be found in Balkwill (1978), Trettin (1989), Trettin and Okulitch (1989) and Okulitch et al. (1990).

The on-shore geology of northeast Ellesmere Island can be divided into four major belts (Fig. 1). The Northern Ellesmere Magmatic Belt (NEMB) is composed mainly of the composite Pearya terrane (Trettin, 1987). Pearya consists of four major successions which range in age from Middle Proterozoic

to Late Silurian. The two successions most relevant to the Lincoln Sea area are: (a) a coastal crystalline basement region of granitoid gneiss with lesser amounts of amphibolite, schist, marble and quartzite (metamorphism and intrusions are dated at 1.0-1.1 Ga) and (b) an Upper Proterozoic to possibly Middle Ordovician succession including sedimentary and volcanic rocks of greenschist to amphibolite metamorphic grade. The sources of the magnetic anomalies are likely to be found in the crystalline basement rocks and in the mafic volcanics and dark clastics of succession (b) (Trettin, 1989). The terrain is rugged with a relative relief of from 1000-2000 m.

A northeast tapering wedge of Sverdrup Basin rocks of the Clements Markham Fold Belt lies southeast of the NEMB. Structural trends are generally NE-SW. In the map area, thick shale and sandstone sequences form the basis for mountainous plateaus with elevations of over 2 km. Diabase dikes and sills characterize the Sverdrup Basin region of Axel Heiberg Island and the northwest corner of Ellesmere Island (Ricketts et al., 1985). Similar intrusive rocks may also be present beneath the Sverdrup Basin region of the survey area.

The Sverdrup Basin is bounded on the south by the Hazen Fold Belt. This terrane is similar in age (Higgins et al., 1982), composition, and terrain to the NEMB. The Hazen Fold Belt is divided by the northeast striking Lake Hazen Fault Zone which trends offshore immediately north of Alert (Fig. 1).

The Central Ellesmere Fold Belt (CEFB) trends NE-SW from the southwest tip of Ellesmere Island to the Judge Daly Promontory. It is characterized by extensive folding and the Judge Daly Fault Zone that runs along Judge Daly Promontory and extends into Robeson Channel (Okulitch et al., 1990; Hood et al., 1985). The CEFB is underlain by limestone carbonates and covered by a layer of turbidites (Hurst and Kerr, 1982). The thickness of this sedimentary layer increases markedly from southeast to northwest (Kerr, 1977).

Three of these four geological belts trend sub-parallel to the northern coast on Greenland (Fig. 1). The Greenland counterpart of the NEMB is found on the northern tip of Peary Land between 40°W and 25°W. This area has rough, mountainous terrain, and is composed of folded Devonian carbonates and

sandstone. It contains a few narrow dikes, predominantly oriented north-south (Soper et al., 1982). The northeastern extent of Sverdrup Basin rocks may underlie the southern Lincoln Sea area.

To the south of Peary Land lies the counterpart of the Hazen Fold Belt. The folds in this region are numerous and complex, and the Harder Fjord Fault crosses the entire region from east-west. There are a great many dolerite dikes in Peary Land, ranging from 25-200 m in thickness, and predominantly oriented north-south. Chemical analysis (Soper et al., 1982) indicates these dikes contain approximately 10% by weight FeO, and 3% Fe_2O_3. Thus, the dikes are extremely magnetic and the magnetic map of this geological province and its extension on Ellesmere Island should provide clues to the region's tectonic history.

South of the counterpart of the Lake Hazen Fold Belt is a 20-30 km wide terrane similar in geology to the CEFB. The folds are not as complex as those to the north, and the thickness of the Devonian sediments decreases to the south. The region is still mountainous with peaks reaching elevations of 1000 m.

In addition to these three geological belts, volcanic rocks known as the Kap Washington Group occur near 40°W on the northwest tip of Peary Land. The age of the Kap Washington Group is estimated at 63 m.y. (Larsen et al., 1978).

3. SURVEY AIRCRAFT SYSTEM - NAVIGATION AND MAGNETICS

The IAR Convair 580 is a research aircraft instrumented for total-field, vertical and horizontal gradient measurements of the aeromagnetic field. Over a number of years the aircraft has been used in cooperative efforts between the GSC and Defense Research Establishment Pacific (DREP). These missions give the IAR the opportunity to maintain the system as both a working survey aircraft and as a developmental platform for aeromagnetics research. At the same time the GSC and DREP benefit from the services of highly developed airborne magnetic and navigation systems.

3.1 NAVIGATION

In addition to magnetic survey capabilities, the aircraft is used as a platform to conduct studies into precise navigation. It has a full complement of navigation systems including:

LTN90 STRAPDOWN INERTIAL SYSTEM	*
CMA-786 C/A CODE GPS RECEIVER	*
GNS 500 VLF-OMEGA RECEIVER	*
DECCA DOPPLER '72	*
VIDEO ON-TOP SYSTEM	*
ARNAV-40 LORAN-C RECEIVER	
DEL NORTE 540 TRANSPONDER SYSTEM	
NORSTAR 1000 GPS P-CODE RECEIVER	@

* = Used in flight guidance for both surveys

@ = Used for track recovery in 1990 survey

None of these navigation systems offers performance that completely meets the accuracy required of the current survey. However, all have complementary characteristics that can help to meet the basic navigation requirements. Thus, for the flight guidance task, a desirable objective was to combine all the navigation data analytically in an optimum fashion, without requiring a great deal of operator intervention or decision making. Since this is a real-time task, a Kalman filter algorithm was chosen. This filter is, in essence, a comprehensive error state model of the inertial system plus Markov error models for the other sensors. Initial estimates of the errors are made and these are refined continuously, based on observations from the non-inertial sensors. The updated estimates of the inertial position errors are applied in a "feed forward" sense to the raw inertial data to give an optimum estimate of position in real time.

Analysis of the navigation data collected during the 1989 survey flights, and run with an off-line version of the filter revealed a flaw in the operation of the Kalman filter, which can be described as follows.

The C/A Code GPS data has a potential accuracy of 25 to 50 metres, which

is considerably better than that of the other radio-based measurement systems used in the survey or similar systems used previously by industry contractors in the south. Similarly, imagery from the vertical on-top system has a potential precision of a few tens of metres. Thus, in the Kalman filter, the error parameters for these two sources of data are such that their data have high authority in the filter. Without valid GPS data or an on-top fix, in the long term the filter will smoothly follow the GNS (VLF) position, with the short-term character of the inertial data. When the GPS is available, the filter will follow it very closely and smoothly, both on the long term and on the short term. When a vertical on-top update becomes available, the filter will move quickly to very close to the new position.

The problem arises when GPS has been available and then is lost, a common occurrence with the current sparse satellite coverage, especially during the 1989 survey. Under this condition, the filter tends to become unstable, failing to revert to following the GNS on the long term as it should. Similarly, the filter can diverge after an on-top update. The divergence is subtle and the filter operated well enough to allow for acceptable flight guidance with few significant errors. The final flight path, determined as part of the post flight processing stage, used the technique described later in this report.

3.2 MAGNETIC INSTRUMENTATION OF THE CONVAIR

The Convair is equipped with three Scintrex VIAW 2125 cesium vapour non-oriented magnetometers, mounted as shown in Figure 2. The Larmor frequencies of the magnetometers are combined as shown in the system block diagram of Figure 3 to form the total-field and gradient signals. Total-field is computed from the average of the wingtip magnetometers and lateral gradient from the difference of these two magnetometers. Longitudinal gradient is computed as the first derivative of total-field divided by measured ground speed. Vertical gradient is measured as the difference between the tail magnetometer and the averaged wing tip magnetometers, with a correction to remove the component of longitudinal gradient introduced by the vertical

"stagger" of the sensors. The effective baselines for the three gradient measurements are shown in Figure 4. Figure 4 also shows the compensated gradients during a series of pitches and rolls on various headings. The gradient quantities are measured in the body axis coordinates of the aircraft and are normally transformed to a horizontal level in the track axis of the survey, using measured aircraft attitudes and drift angle.

The bandwidth of all Larmor-derived and analog signals is from 0 to 1.67 Hz, set by carefully matched anti-aliasing filters. At an average aircraft speed of 110 m/sec, this translates to an along-track sampling resolution of approximately 66 metres.

Compensation (in which the aircraft magnetic interference is modelled and corrected for) is possibly the most critical element in the on-line processing of aeromagnetic data. Poor compensation can lead to levelling errors in total-field gridding. For the horizontal gradients, good compensation is exceedingly important in that when these data are used to enhance the total-field presentation, small, compensation-related errors can considerably distort the final product.

Compensation coefficients are calculated by doing a set of manoeuvres (called a "Figure of Merit", or "FOM") in a region of low, uniform gradient within, or not greatly removed from, the survey area. Great care is taken to prevent changes to the magnetic signature of the aircraft during the course of the survey. To monitor possible changes with time and ensure consistency, an FOM is flown at the end of the survey and four-heading checks are flown in low-gradient areas of opportunity on a daily basis.

In the Convair system (Fig. 3), three sets of compensation coefficients are used, for total-field (TF), lateral gradient (GY), and vertical gradient (GZ) respectively. The compensation terms are linear combinations of the aircraft's direction cosines with respect to the earth's field vector, as measured by the vector magnetometer; they are the same for each "axis" of compensation. The interference model used for real-time (on-line) compensation consists of 28 such terms, three for permanent magnetism, six for induced, 18 for eddy current fields and one term to compensate for orientation error in the non-oriented ("strapdown") cesium magnetometers.

3.3 GROUND BASED STATION

A cesium vapour magnetometer was set up as a base station magnetometer in order to measure and record background magnetic field changes during the survey. These data were sampled and recorded at high sampling rates (3.6 Hz in 1989 and 8.0 Hz in 1990) and the time synchronization with the aircraft system clock was within 1 second. The base station was established at the seismic vault maintained by the GSC at Alert away from the main operations, so the magnetic data are not subject to cultural noise. Base station data were used to monitor the background field and confirm that the flight data were not significantly affected by diurnal changes during the survey.

As part of the ground station operations, a first-look data confirmation capability exists that allows for daily examination of the data recorded in-flight. After each day's operations the flight data tape (which is the primary data storage medium) was read and selected data fields (magnetics and navigation quantities) were demultiplexed and written to disk on a portable computer. These data were then plotted and examined in order to identify any problems in the aircraft system prior to the next survey flight. These plots were used to select low gradient areas for locating the magnetic tie lines.

4. DATA ACQUISITION AND POST FLIGHT PROCESSING

4.1 ACQUISITION

The area to be surveyed was defined in 1988 by the GSC and DREP due to its importance in placing constraints on: (i) the existence of major tectonic structures between Ellesmere Island and Greenland and (ii) the nature of continental breakup and ocean ridge and basin formation in the area between the Alpha and Lomonosov Ridges. The area had not been adequately covered by previous aeromagnetic work, although some widely spaced survey lines were flown by the US Navy in 1975 (Kovacs, 1982; Kovacs and Vogt, 1982). The survey grid that was defined to cover the area was centred on longitude

57.5°W; all survey lines were to be parallel to this meridian spaced at 4.0 km, and extend from 82.0°N to 84.5°N (at the meridian). In order to cover the area a total of 77 lines was specified. To date 68 lines have been flown, 37 in 1989 and 31 in 1990. Four tie lines were flown perpendicular to the 1989 survey lines and a different 4 tie lines were flown roughly perpendicular to the 1990 set of lines. These tie lines were selected to run through low gradient areas, by examination of the preliminary total magnetic field plots that were produced daily while the aircraft was on site.

All lines flown over water were flown at an altitude of 300 m. Over land, most of the lines were flown in a "draped mode" with a vertical separation of 300 m. Due to topography and safety considerations however, a few lines over land were flown at a constant altitude of 6500 m.

The specifications for this survey were very challenging given the remote offshore environment. However, the productivity achieved per day at the site was quite high. During the 1989-1990 operations an average of 775 line kilometres per day on site were surveyed. This compares very favourably to past Arctic surveys to the south sponsored by the GSC. For any aeromagnetic operations in the Arctic the dominant factors influencing productivity are inclement weather and an active external field, which no amount of forward planning can entirely account for.

4.2 POST FLIGHT PROCESSING

The post flight data handling consisted of three distinct phases. Immediately after each flight, field plots (described in section 3.3) were created of the flight path and the total magnetic field. After returning from the field the data were subject to a more in-depth but still preliminary analysis (at DREP), the result of which are the total-field plots that are included with this report.

Concurrent to this analysis, a series of final data processing steps were being prepared by the IAR. The first processing pass is a serial operation on the flight format tape in order to identify occasional gaps in the data that were most often caused by repeated magnetic tape drive write

failures. When the gaps are lengthy (more than a few blocks long) the problem is normally associated with a computer system failure. In these cases the flight line would have been broken off and restarted, possibly resulting in small gaps in the data. When the gaps are very short, a gap-filling routine is applied since some of the subsequent processes require continuous data segments. Infilling is done by demultiplexing the field tape, by fitting splines to each channel and by re-sampling these splines across the gaps. After infilling, the data are written to a series of files on disk for further processing.

Although the real-time compensated data are of a high quality (the preliminary analyses done by DREP used these data), there are some recent enhancements, applicable particularly to gradient compensation, that have not yet been incorporated into the on-line algorithm. Thus, to ensure the very best results, the magnetic data have been recompensated off-line. These additional features include:

- More robust coefficients by combining more than one FOM data set.
- Three additional terms to take into account the local residual gradient of the area where compensation data are collected. (This is particularly important for the lateral gradient).
- Trimming the DC baseline of the lateral and vertical gradients.

In the last item, gradient measurement, the DC value (or DC "baseline") is very important, but its value is difficult to stabilize; very small changes in the aircraft's magnetism cause large changes in the baseline. Furthermore, recent investigations indicate what appear to be hysteresis effects in the ferromagnetic materials interfering with the gradiometer signals. These materials retain their magnetization from the last line (flown in the opposite direction), resulting in a shift of DC baseline from line to line. Such non-linear effects are difficult to deal with in the linear compensation algorithms. For the 1989 data, an interim solution was to scan the magnetic data of each line to find an area of minimum gradient and then to zoom in on this portion of the line to find a small section in which

there is roll-axis activity where the flight path was being corrected to maintain track. Such adjustments usually require about 3 to 4 degrees of bank. This small manoeuvre is used to compensate the transverse and longitudinal permanent terms (T and L) and these "trimmed" values are then applied to the entire line. This trimming overcomes any line-to-line baseline shift in the lateral gradient and has the further advantage of greatly reducing residual interference from the small roll manoeuvres. This latter interference arises from the fact that at very high dip angles (near 90 degrees for Lincoln Sea), T and L are very difficult to identify and separate from crosstalk caused by the aircraft manoeuvring in a non-zero vertical gradient (Fig. 4).

In the 1990 survey, as each line was flown, several deliberate 5 degree rolls were done in a minimum gradient area. Thus, it was not necessary to scan the data for rolls occurring in low gradient areas.

The vertical gradiometer in the Convair is compensated to an average noise level of 30 to 40 pT/m over the maximum manoeuvre envelope of the aircraft (Fig. 4). Because of very high interference at the tail magnetometer, a lower noise figure is difficult to achieve. In most of the Lincoln Sea survey, the target sources are roughly 1 km below the 300 m survey altitude, giving very weak vertical gradient signals that are in many cases at or below the noise level. In summary, the vertical gradient data appear to be noisy, but given the depth of the sources and the line spacing, it is unlikely that the vertical gradient would be useful in delineating the basement structures. As is the case with the lateral gradient, the vertical gradient is subject to DC baseline shifts, but little effort has been made to level these baselines. For this reason, the attitude decoupling of the gradients, shown as the last operation before gradient output in Figure 3, was not done completely; the body-axis longitudinal and lateral gradients were simply translated into the track axis of the survey. However, as stated previously, the T and L trimming effectively eliminates the vertical gradient crosstalk in the lateral gradient signal.

The navigation data underwent a series of quite separate processes aimed at generating a "best estimate" of flight path. The flight guidance is

handled by an error state Kalman Filter process that attempts to model and correct INS errors (the system plant). The filter has certain advantages in the real time environment in which it operates and normally results in an improvement over the raw GNS, INS, or Doppler information. However, as explained in section 3.1, in cases when the filter has been updated by an accurate measurement (such as GPS or an on-top) and then these data cease to be available, the filter may become unstable and results diverge.

The instability is subtle and was only fully characterized after the 1990 survey. It is fortunate that the instability is usually relatively weak and the guidance was generally acceptable. During the 1989 survey, there were a few occasions when a divergence became obvious through inspection of raw position difference data on the system screen display. Fortunately, on these occasions, the problem was noticed early enough and the guidance was changed from the filter to the system whose raw data were judged best before significant track error had occurred. In 1990, the problem of filter instability was virtually non-existent because it was nearly always possible to arrange the survey on-line times to coincide with GPS satellite coverage.

For these reasons and since the Kalman Filter is recursive, it is not ideally suited to the off-line flight path recovery tasks, in which both past and future data are available. As an alternative, this was accomplished by fitting, in a weighted least squares sense, an INS function to the INS-GNS, INS-on-top and INS-GPS difference functions. In those cases in which GPS coverage was available throughout a flight, the GPS was used to model the INS errors. Separate error functions have been generated for the INS latitude and the longitude for each flight. The error functions were then subtracted from the INS time series to yield corrected INS which is the final flight path. This process is illustrated by Figure 5.

The final archive data set is made up of four files per flight; one each of magnetics, navigation, altimeter, and magnetic base station. Each file is flat, each record within each file is time stamped, and each file has its own characteristic data rate.

4.3 ANALYSIS OF THE TOTAL-FIELD DATA

Only the total-field data have been analysed in this report. The gradient data will be analysed at a later date. Figure 6a shows the flight line and tie line coverage. The raw total-field profile data are shown in Figure 6b for the 1989 data and Figure 6c for the 1990 data. No downward continuation processing was applied to the lines over land flown at 6500 m.

Total-field contour maps were produced from 1 Hz subsampled aeromagnetic data, and 1 Hz (interpolated) navigation data. Levelling was accomplished by the technique outlined below and gridding was done with an iterative Laplace polynomial interpolation algorithm implemented in the data analysis program "MAGIC" at DREP.

To level the data a crossing point error was defined as the field measured along the survey line minus the field measured along the tie line at the intersection of the survey and tie line. The crossing point errors were linearly interpolated between crossing points along each survey line. A constant error, equal to the first crossing point error, was assumed between the first data point along a survey line and the first crossing point on that survey line. Similarly, a constant error equal to the last crossing point error was assumed between the last crossing point and the last data point along a survey line. In this way, an error profile made up of constant values and trends was calculated for each survey line. These error profiles were then subtracted from the corresponding raw total-field profiles along the survey lines.

Some researchers have successfully levelled high-latitude aeromagnetic surveys with a combination of ground station subtraction and trend removal (Skilbrei et al., 1990). Unfortunately, the ground station at Alert was situated on a large conductivity anomaly (Niblett et al., 1974) which distorts the phase of variations in the Earth's magnetic field. Thus a disturbance in the Earth's field measured at Alert does not have the same characteristics when measured above the Lincoln Sea. However, we are presently investigating alternate techniques to improve the levelling, including ground station subtraction.

The 1989 and 1990 data sets were analysed individually. Figure 7 is a surface plot of the entire data set (1989 and 1990) produced by merging the

two levelled gridded data sets, and Figure 8 is a grey-scale contour plot of the same data.

5. INTERPRETATION

5.1 GENERAL FEATURES

The dominant features on Figures 7 and 8 have been labelled A-H. The magnetic characteristics of each feature are described below.

There is a significant difference in the regional nature of the magnetic field anomaly pattern from the complex field north of Ellesmere Island to the relatively flat area north of Greenland (Fig. 6a and Fig. 6b). There is also a change in the higher frequency anomaly trends from northeast, between Ellesmere Island and Greenland, to east-west north of Ellesmere Island to northwest in the northwest corner of the area (Fig. 6a).

Area A features a high amplitude anomaly with a wavelength of about 25 km amidst a group of anomalies characterized by a wavelength of 5-10 km and peak amplitudes of 300-400 nT similar to those in area B. Assuming the bathymetry is correct, the higher frequency anomalies reflect relatively shallow sources beneath the continental shelf-slope.

The NW-SE trending linear features in area B appear to represent the southwest corner of an anomalous area of short-wavelength anomalies described by Kovacs (1982). The anomalies are characterized by a wavelength of 5-10 km and peak amplitudes of 300-400 nT. The magnetic anomalies are very different from those of the Alpha Ridge to the west, the Lomonosov Ridge to the northeast, and the Lincoln Sea to the south (Forsyth et al.,1990).
The E-W linear trends of large-amplitude, short-wavelength anomalies labelled C suggest shallow intrusive sources.

Area D contains a band of low-amplitude, longer-wavelength anomalies trending ENE. These anomalies are about 40 km north of Alert and appear to be an offshore continuation of the northeast tapering wedge of Sverdrup Basin rocks (Fig. 1).

E contains a group of short-wavelength anomalies aligned with the centre

of Robeson Channel as it enters the Lincoln Sea. The Robeson Channel anomalies appear as a continuation of the Judge Daly Fault Zone from Judge Daly Promontory (Fig. 1). It is clear that these anomalies do not continue in a straight line out into the Lincoln Sea, and thus do not clearly support the proposed Wegener Fault (Kovacs, 1989).

The central survey area F, is characterized by small-amplitude, high-frequency anomalies superimposed on small-amplitude, longer wavelength anomalies (Fig. 6c).

G contains several E-W trends of low-amplitude, high-frequency anomalies (Fig. 6c, L60-66). The anomalies on lines 76 and 77 (not plotted in Fig. 7) suggest the start of more interesting structure to the east and will be included with the analysis of data following completion of the 1991 survey.

Finally, the northeast corner of the survey area (H) contains low-amplitude anomalies with wavelengths of 15-30 km trending roughly E-W, parallel to the north Greenland shore.

5.2 DEPTH-TO-MAGNETIC SOURCE

For depth-to-source analysis, the total-field profiles were subsampled to 1 Hz (approximately 110 m sample spacing). Individual anomalies from the profile data were analysed with "MAGMOD3", a commercial software package from Geosoft Inc. This program calculates the magnetic and geometric parameters of a thin dike, an infinite extent tabular body, or a finite extent tabular body, by a least-squares comparison to the measured anomaly. The program assumes that the aircraft track was perpendicular to the strike, and directly over the centre, of the causative body. In addition, some anomalies were analysed with the half-slope method (Rao and Babu, 1984) to determine depth-to-source. Figure 9 is a map of the survey area with the estimated depth-to-source shown at the location of the anomaly analysed.

In area A, the large-amplitude, low-frequency anomaly near x=40 km; y=220 km is caused by a source which is estimated at 5 km below the sea surface. However, just north of this anomaly, the sources depths are estimated at 1-2 km. Because the bathymetry is about 1 km, these sources are

near the sea-floor and covered with less than 1 km of sediments.

The NE-SW trending band of anomalies in area B are estimated to have source depths of approximately 2.5 km. Bathymetry in this region is 1 km, which indicates a sediment cover of about 1.5 km.

The high-frequency, large-amplitude anomalies in C are probably due to intrusive dikes which typically lie some 300-800 m below the sea surface. The bathymetry is only 200 m in this area so the intrusions almost reach the sea-floor.

The anomalies in area D yield depths to source of 100-700 m. Because the bathymetric values in this area are approximately 100 m, most of these sources lie within 600 m of the sea-floor.

The band of anomalies in Robeson Channel and just offshore of Greenland's northern coast (E) have source depths which vary from 400-800 m. The bathymetry varies from 300-500 m, indicating a sediment cover of only a few hundred metres at most.

Area F is characterized by high-frequency, low-amplitude anomalies and low-frequency, low-amplitude anomalies. Depth estimates from the high-frequency anomalies ranged from 0-700 m, while the bathymetry ranges from 0-500 m. This indicates that these sources are very near the sea bottom. Because the amplitudes of these anomalies are low, either the sources are physically small or the magnetization of the material is low. The ratio of the peak amplitudes above the suggested dikes in area C to those of the low-amplitude, high-frequency anomalies is about 50-100. This indicates that either the magnetization of this material is a factor of about 50-100 times less than that of the dike material, or the physical size of the sources is 50-100 times smaller.

Depth-to-source analysis was difficult to perform on the low-frequency anomalies in area F. However, two anomalies on line "L51" yielded depth estimates of approximately 12000 m.

G contains a series of anomalies which yield depth estimates of 300-1000 m. Bathymetry in this region ranges from 0-500 m, indicating some 500 m of sediment may be present.

Finally, the anomalies in H are low-frequency. Depth estimates range

from 2000-7000 m, with an average value of about 5000 m. Bathymetry in this region varies from 1000-2000 m, indicating sediment depths of about 3000-4000 m.

6. CONCLUSIONS

The 1989 and 1990 Lincoln Sea surveys have demonstrated that relatively detailed aeromagnetic surveying can be achieved in the high Arctic with the available navigational resources. In addition to acquiring high quality data, the 1989 and 1990 surveys have included testing and developmental components with the aim of improving future missions. Navigational precision will increase and post-processing requirements will decrease as the high latitude GPS coverage improves.

Many new magnetic features with unknown geological and tectonic significance have been identified in the preliminary magnetic data. Although many of the depth-to-source estimates generally agree with those of Kovacs (1982), this survey defines anomaly wavelengths, directions and strike length that have not been quantified before. The high-frequency anomalies from probably shallow sources in region F have not been reported nor has the nature and extent of the high amplitude anomalies beneath the shelf north of Ellesmere been defined. A full appreciation of the geological and tectonic significance of the anomaly trends, such as the termination of the high frequency anomaly trends at the mouth of Robeson Channel and the generally smooth character of the eastern Lincoln Sea will require further study.

7. FUTURE WORK

It is hoped that the nine survey lines remaining in the Lincoln sea survey may be completed in April/May 1991. In addition, an aeromagnetic survey extending from Ellef Ringes Island to Ellesmere Island (79°-82°N, 88°-106°W) is planned for 1991-1993. This coincides with the area of the 1985, 1986 and 1990 Ice Island refraction surveys.

Improved levelling procedures using both ground station data and first-

order levelling methods are being investigated at DND and GSC. These procedures will be used when final navigation data are available.

A final map of the area will be produced when the survey has been completed and all optimal navigation data are available.

8. ACKNOWLEDGEMENTS

The authors would like to thank the flight crew, ground crew, and technical support staff of the Convair 580 program at IAR for collecting these data under very difficult conditions. Constructive critiques of the manuscript and significant improvements were received from A.G. Green, M. Pilkington and P. Keating. We are grateful for the support and encouragement received from Dr. Robin Riddihough, GSC Chief Scientist.

9. REFERENCES

Balkwill, H.R., 1978. Evolution of Sverdrup Basin, Arctic Canada, Bull. of the Am. Ass. of Pet. Geol., 62, 1004-1028.

Forsyth, D.A., Broome, J., Embry, A.F., and Halpenny, J., 1990. Features of the Canadian Polar Margin, in J.R. Weber, D.A. Forsyth, A.F. Embry, and S. Blasco (Editors), Marine Geology, 93, 147-177.

Hardwick, C.D., Nelson, J.B., Thorning, L., Bower, M.E., Marcotte, D.L., Forsyth, D.A., Macnab, R., and Teskey, D., 1990. Procedures and preliminary results of an aeromagnetic survey in the Lincoln Sea, Current Research Part D, Geological Survey of Canada Paper 90-1, 11-16,.

Higgins, A.K., Mayr, U., and Soper, N.J., 1982. Fold belts and metamorphic zones of northern Ellesmere Island and North Greenland, in P.R. Dawes and J.Wm. Kerr (Editors), Nares Strait and the drift of Greenland: a conflict in plate tectonics, Meddelelser om Gronland, Geoscience 8, 159-166.

Hood, P.J., Bower, M.E., Hardwick, C.D., and Teskey, D., 1985. Direct geophysical evidence for displacement along Nares Strait (Canada-Greenland) from low-level aeromagnetic data: a progress report, Geological Survey of Canada Current Research paper 85-1A, 517-522.

Hurst, J.M., and Kerr, J.Wm., 1982. Upper Ordovian to Silurian facies patterns in eastern Ellesmere Island and western North Greenland and their bearing on the Nares Strait linament, in P.R. Dawes and J.Wm. Kerr (Editors), Nares Strait and the drift of Greenland: a conflict in plate tectonics, Meddelelser om Gronland, Geoscience 8, 137-145.

Kerr, J.Wm., 1977. Cornwallis Fold Belt and the mechanism of basement uplift, Can. J. Earth Sci., 14, 1374-1401.

Kovacs, L.C., 1982. Motion along Nares Strait recorded in the Lincoln Sea: aeromagnetic evidence, in P.R. Dawes and J.Wm. Kerr (Editors), Nares Strait and the drift of Greenland: a conflict in plate tectonics, Meddelelser om Gronland, Geoscience 8, 275-290.

Kovacs, L.C., and Vogt, P.R., 1982. Depth-to-magnetic source analysis of the Arctic Ocean Region, Tectonophysics, 89, 255-294.

Larsen, O., Dawes, P.R., and Soper, N.J., 1978. Rb/Sr age of the Kap Washington Group, Peary Land, North Greenland, and its geotectonic implication, Rapp. Groenlands geol. Unders, 90, 115-119.

Niblett, E.R., DeLaurier, J.M., Law, L.K., and Plet, F.C., 1974. Geomagnetic variation anomalies in the Canadian Arctic I. Ellesmere Island and Lincoln Sea, J. Geomag. Geoelectr., 26, 203-221.

Okulitch, A.V., Dawes, P.R., Higgins, A.K., Soper, N.J. and Christie, R.L. 1990: Towards a Nares Strait solution: Structural studies on southeastern Ellesmere Island and northwestern Greenland. Marine Geology, 93, 369-384.

Rao, D.A., and Babu, H.V.R., 1984. On the half-slope and straight-slope methods of basement depth determination, Geophys., 49, 1365-1368.

Ricketts, B.D., Osadetz, K.G., and Embry, A.F., 1985. Volcanic style in the Strand Fiord Formation (Upper Cretaceous), Axel Heiberg Island, Canadian Arctic Archipelago, Polar Research, 3, 107-122.

Skilbrei, J.R., Habrekke, H., Christoffersen, T., and Myklebust, R.,1990. Aeromagnetic surveying at high latitudes, a case history from the northern Barents Sea, First Break, 8, 46-50.

Soper, N.J., Dawes, P.R., and Higgins, A.K., 1982. Cretaceous-Tertiary

magmatic and tectonic events in North Greenland and the history of adjacent ocean basins, in P.R. Dawes and J.Wm. Kerr (Editors), Nares Strait and the drift of Greenland: a conflict in plate tectonics, Meddelelser om Gronland, Geoscience 8, 205-220.

Trettin, H.P., 1987. Pearya: a composite terrane with Caledonian affinities in northern Ellesmere Island, Can J. Earth Sci., 24, 224-245.

Trettin, H.P., 1989: The Arctic Islands; in Bally, W.A. and Palmer, A.R. (Editors), The Geology of North America-an overview: Boulder Colorado, Geological Society of America, The Geology of North America, Vol. A, 349-369.

Trettin, H.P. and Okulitch, A.V., 1989: Tectonic framework, Canadian Arctic islands and north Greenland; International Geological Congress, 28th (Washington, D.C.), 3, 250-251.

FIGURE CAPTIONS

Figure 1. Generalized geological map of northern Ellesmere Island, northern Greenland, and the Lincoln Sea. Survey area is outlined.

Figure 2. Location of magnetometers in the Convair 580.

Figure 3. Block diagram of the Convair 580 magnetic data acquisition system.

Figure 4. Compensated gradients during manoeuvres.

Figure 5. INS-GNS, INS-GPS, and INS-on-top latitude error functions for flight A8921.

Figure 6(a). Survey and tie line coverage.

Figure 6(b). Raw total-field profiles vs latitude for the 1989 data.

Figure 6(c). Raw total-field profiles vs latitude for the 1990 data.

Figure 7. Surface plot of the gridded (1989 + 1990) total-field data.

Figure 8. Contour plot of the gridded (1989 + 1990) total-field data. Units are nT. Altitude = 300 m.

Figure 9. Estimated depths to sources. Dashed bathymetry in metres.

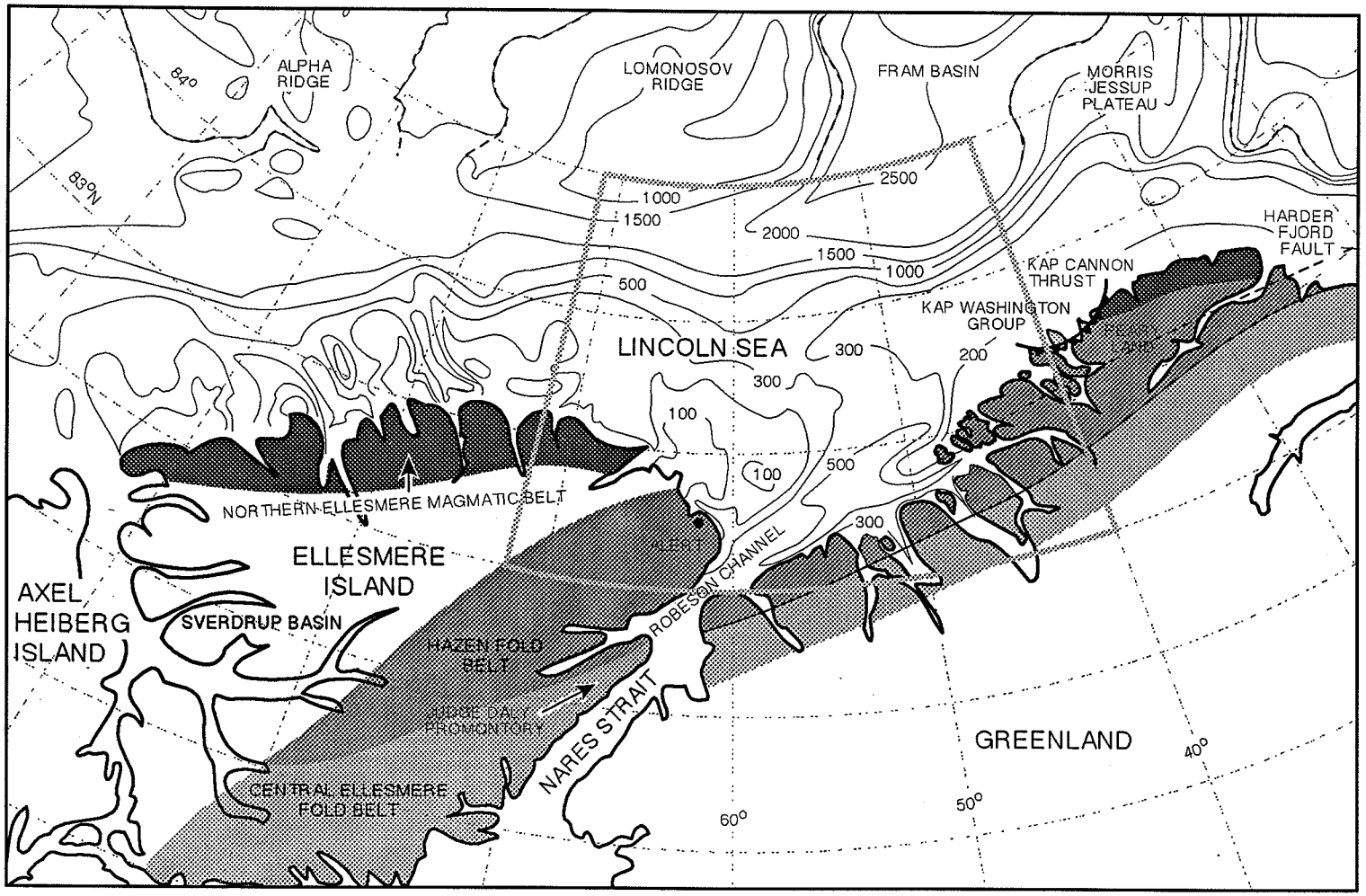
ALPHA RIDGE
LOMONOSOV RIDGE
FRAM BASIN
MORRIS JESSUP PLATEAU
84°
83°N
1000
1500
2000
2500
1500
1000
500
HARDER FJORD FAULT
KAP CANNON THRUST
KAP WASHINGTON GROUP
LINCOLN SEA
300
200
300
100
100
500
300
NORTHERN ELLESMERE MAGMATIC BELT
ELLESMERE ISLAND
AXEL HEIBERG ISLAND
SVERDRUP BASIN
HAZEN FOLD BELT
ROBESON CHANNEL
NARES STRAIT
GREENLAND
CENTRAL ELLESMERE FOLD BELT
60°
50°
40°

Figure 1

Figure 2

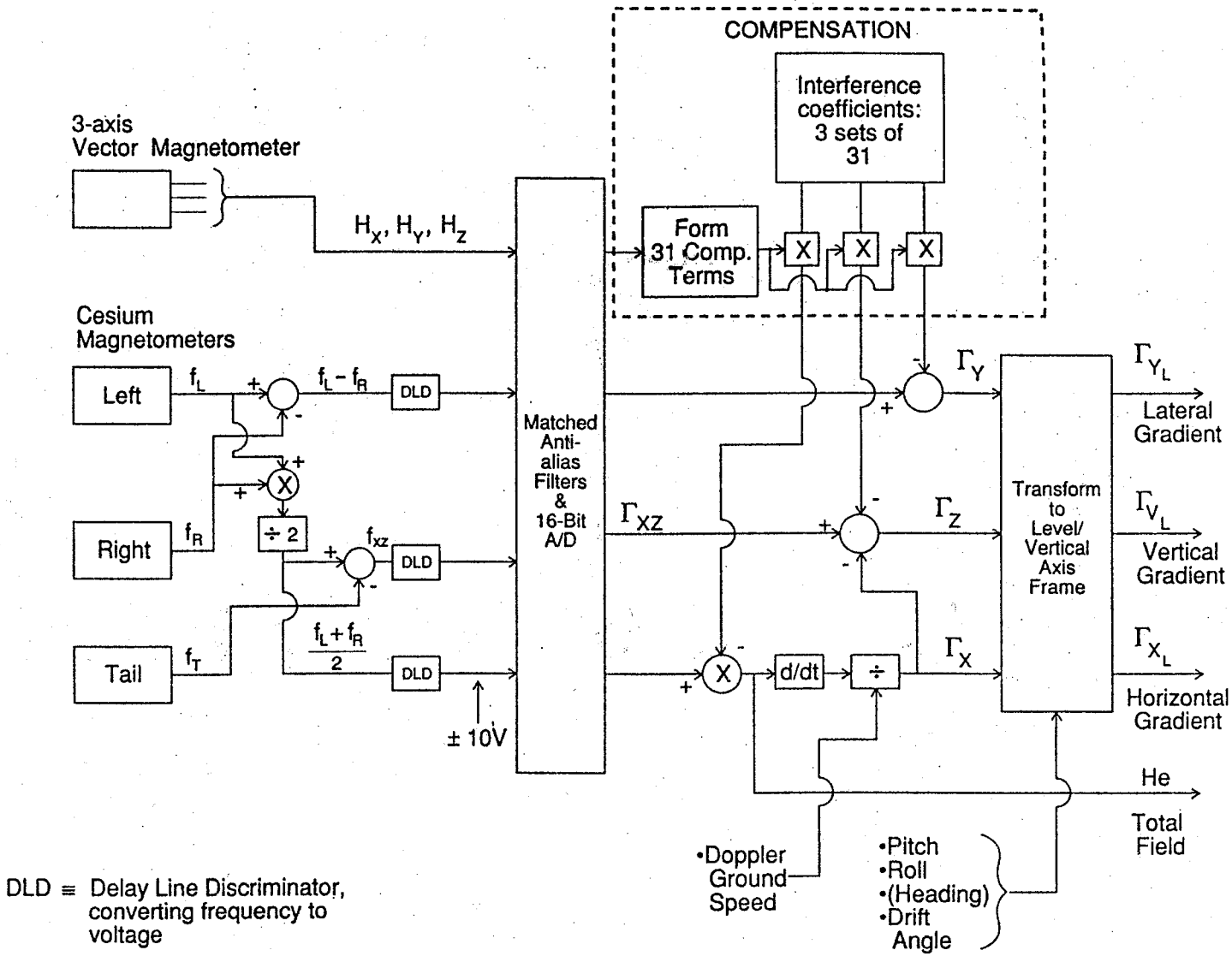

DLD ≡ Delay Line Discriminator, converting frequency to voltage

Figure 3

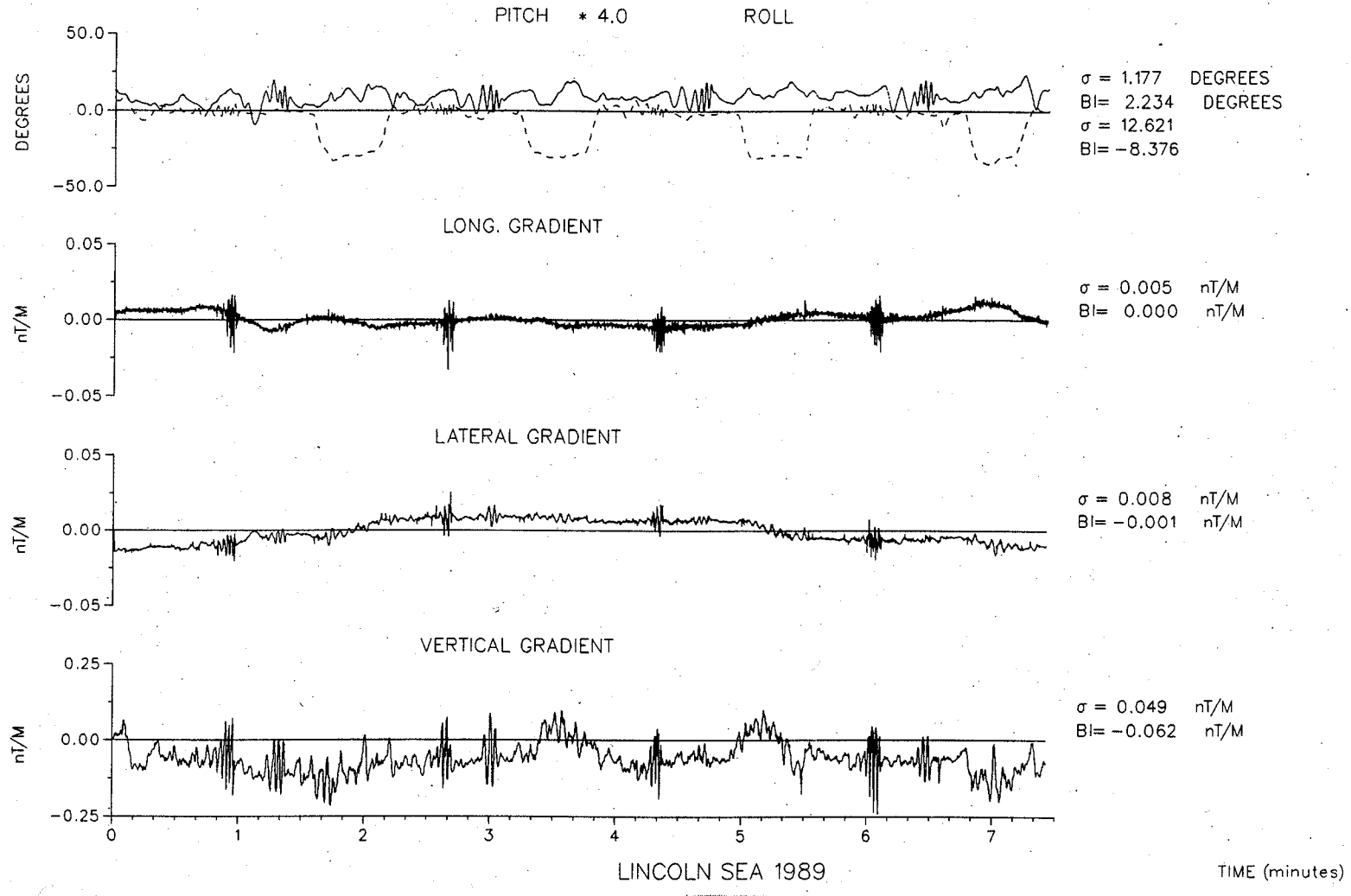
PITCH * 4.0
ROLL
50.0
0.0
-50.0
DEGREES
σ = 1.177 DEGREES
BI= 2.234 DEGREES
σ = 12.621
BI= -8.376
LONG. GRADIENT
0.05
0.00
-0.05
nT/M
σ = 0.005 nT/M
BI= 0.000 nT/M
LATERAL GRADIENT
0.05
0.00
-0.05
nT/M
σ = 0.008 nT/M
BI= -0.001 nT/M
VERTICAL GRADIENT
0.25
0.00
-0.25
nT/M
σ = 0.049 nT/M
BI= -0.062 nT/M
0
1
2
3
4
5
6
7
LINCOLN SEA 1989
TIME (minutes)

Figure 4

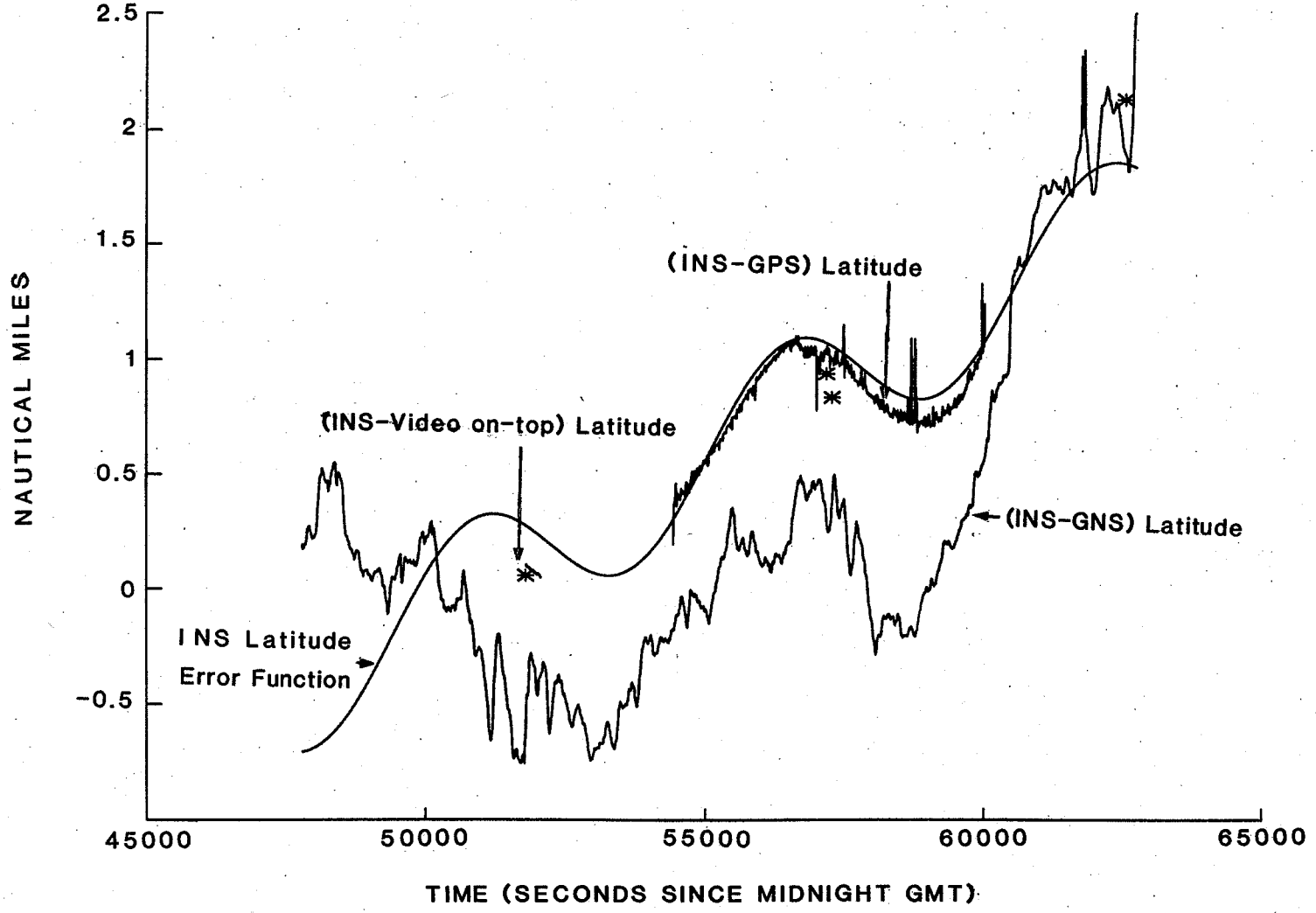
2.5
2
1.5
1
0.5
0
-0.5
NAUTICAL MILES
(INS-GPS) Latitude
(INS-Video on-top) Latitude
(INS-GNS) Latitude
INS Latitude
Error Function
45000
50000
55000
60000
65000
TIME (SECONDS SINCE MIDNIGHT GMT)

Figure 5

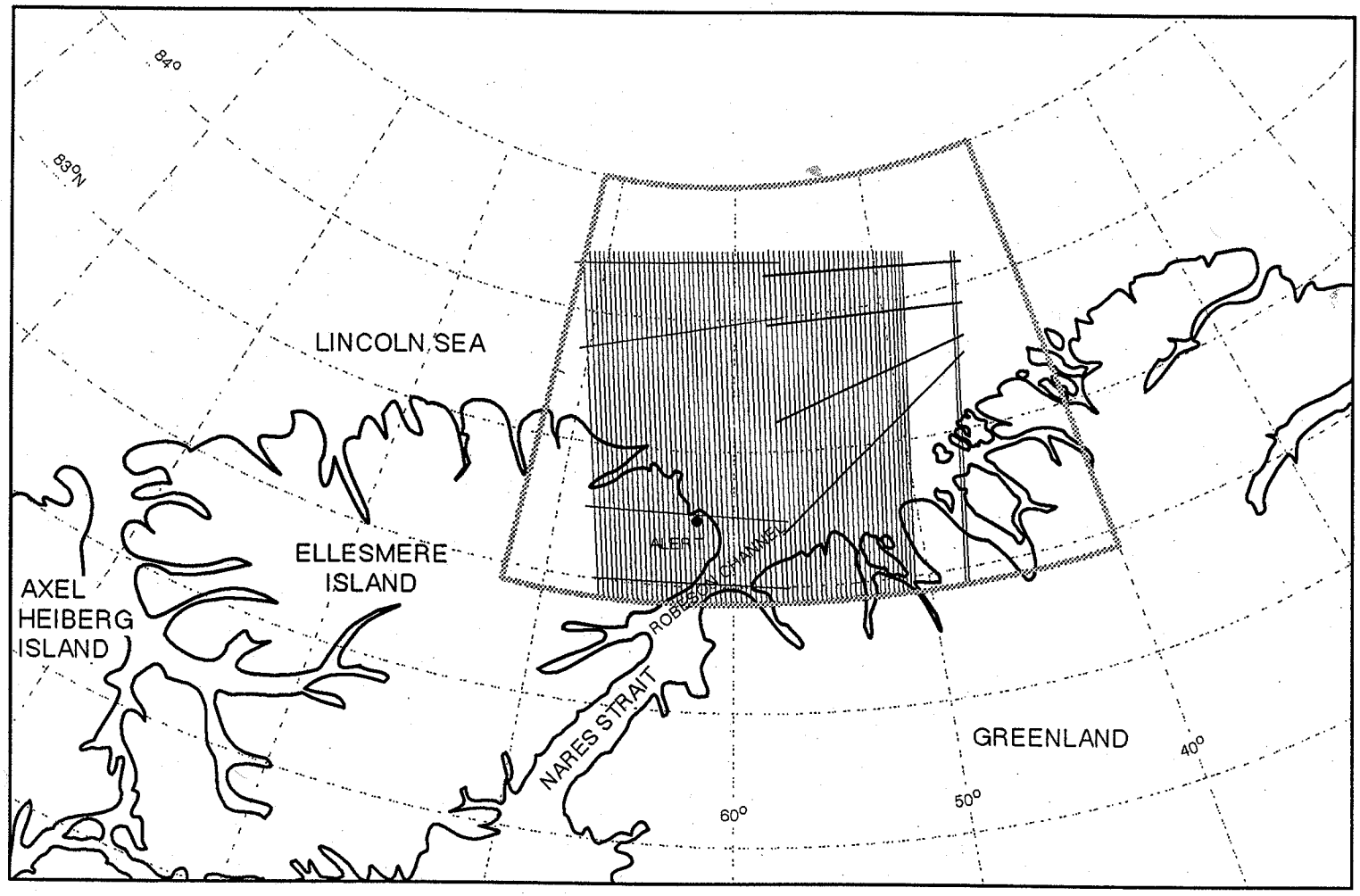
84°
83°N
LINCOLN SEA
ELLESMERE ISLAND
AXEL HEIBERG ISLAND
ALERT
ROBESON CHANNEL
NARES STRAIT
GREENLAND
60°
50°
40°

Figure 6(a)

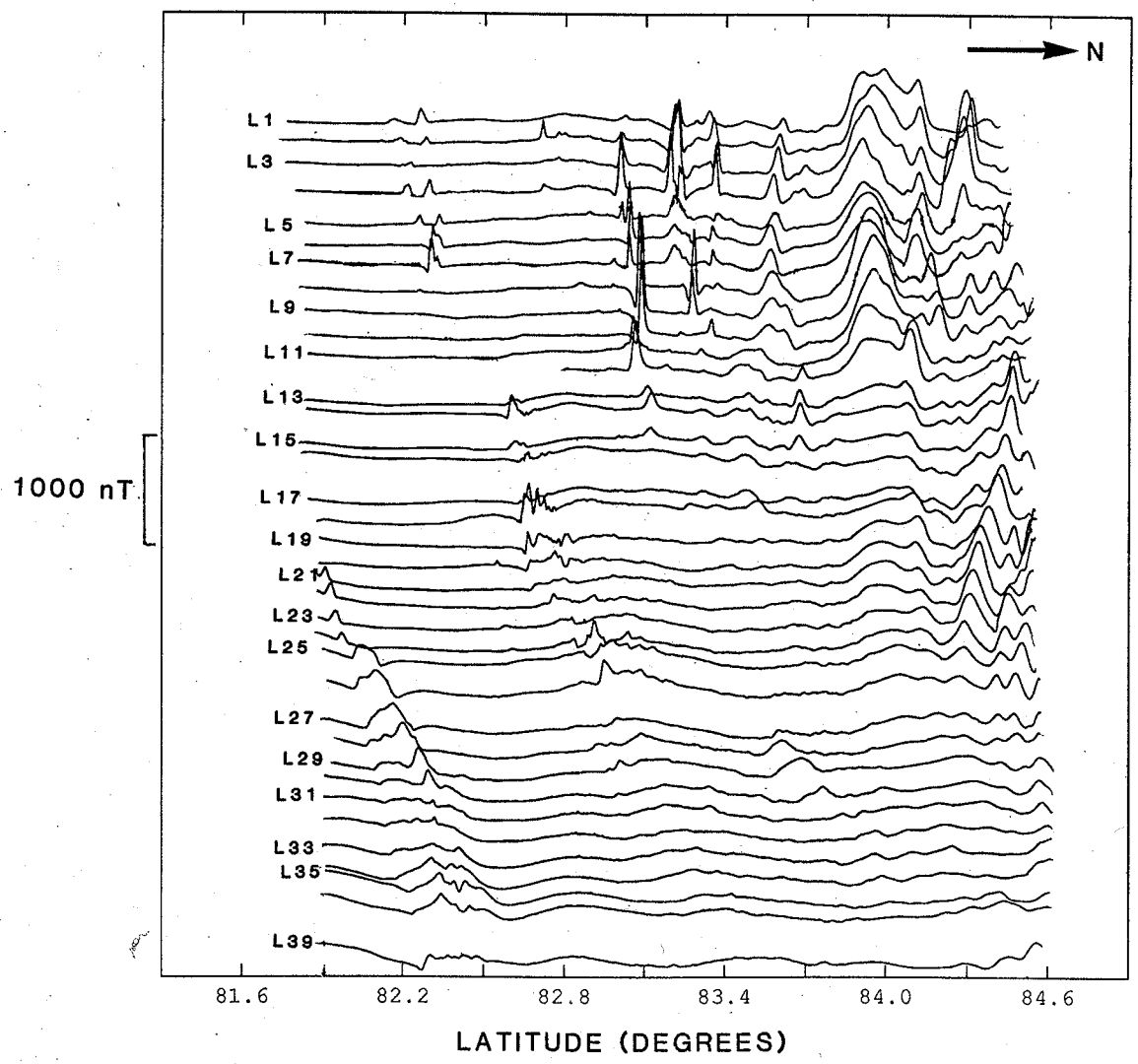
N
L1
L3
L5
L7
L9
L11
L13
L15
L17
L19
L21
L23
L25
L27
L29
L31
L33
L35
L39
1000 nT
81.6
82.2
82.8
83.4
84.0
84.6
LATITUDE (DEGREES)

Figure 6(b)

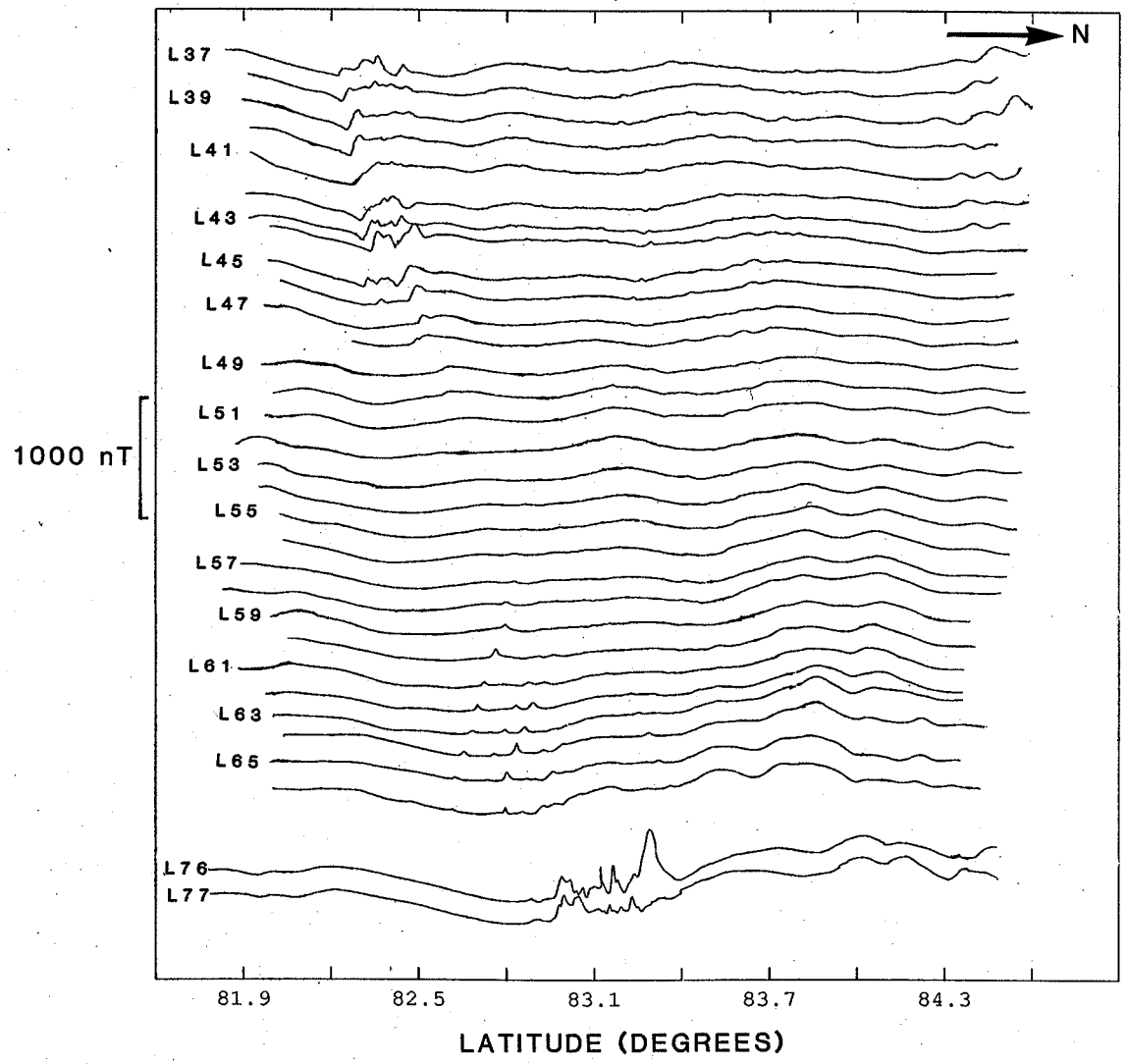
N
L37
L39
L41
L43
L45
L47
L49
L51
L53
L55
L57
L59
L61
L63
L65
L76
L77
1000 nT
81.9
82.5
83.1
83.7
84.3
LATITUDE (DEGREES)

Figure 6(c)

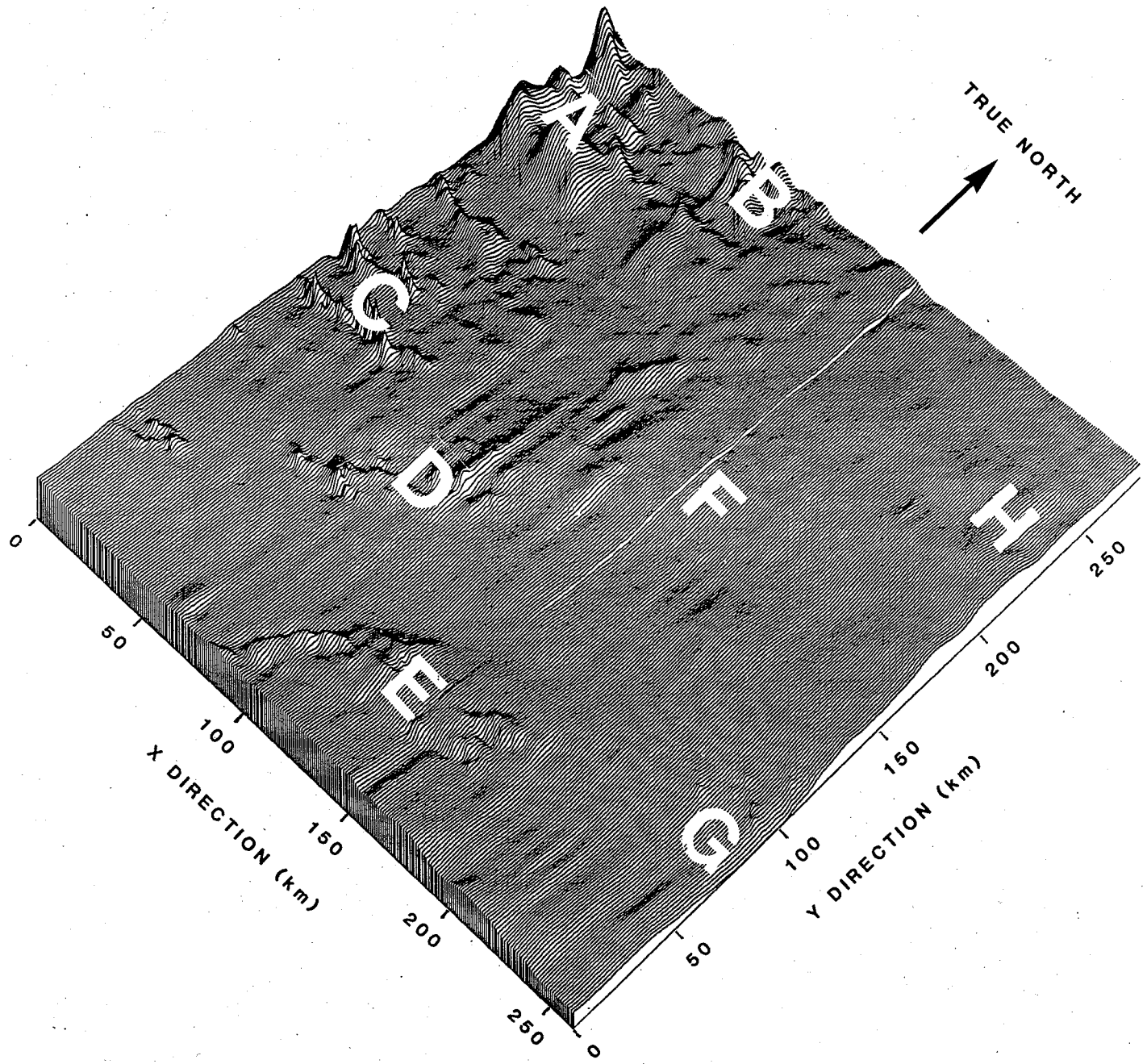
A
B
C
D
E
F
G
H
TRUE NORTH
0
50
100
150
200
250
X DIRECTION (km)
0
50
100
150
200
250
Y DIRECTION (km)

Figure 7

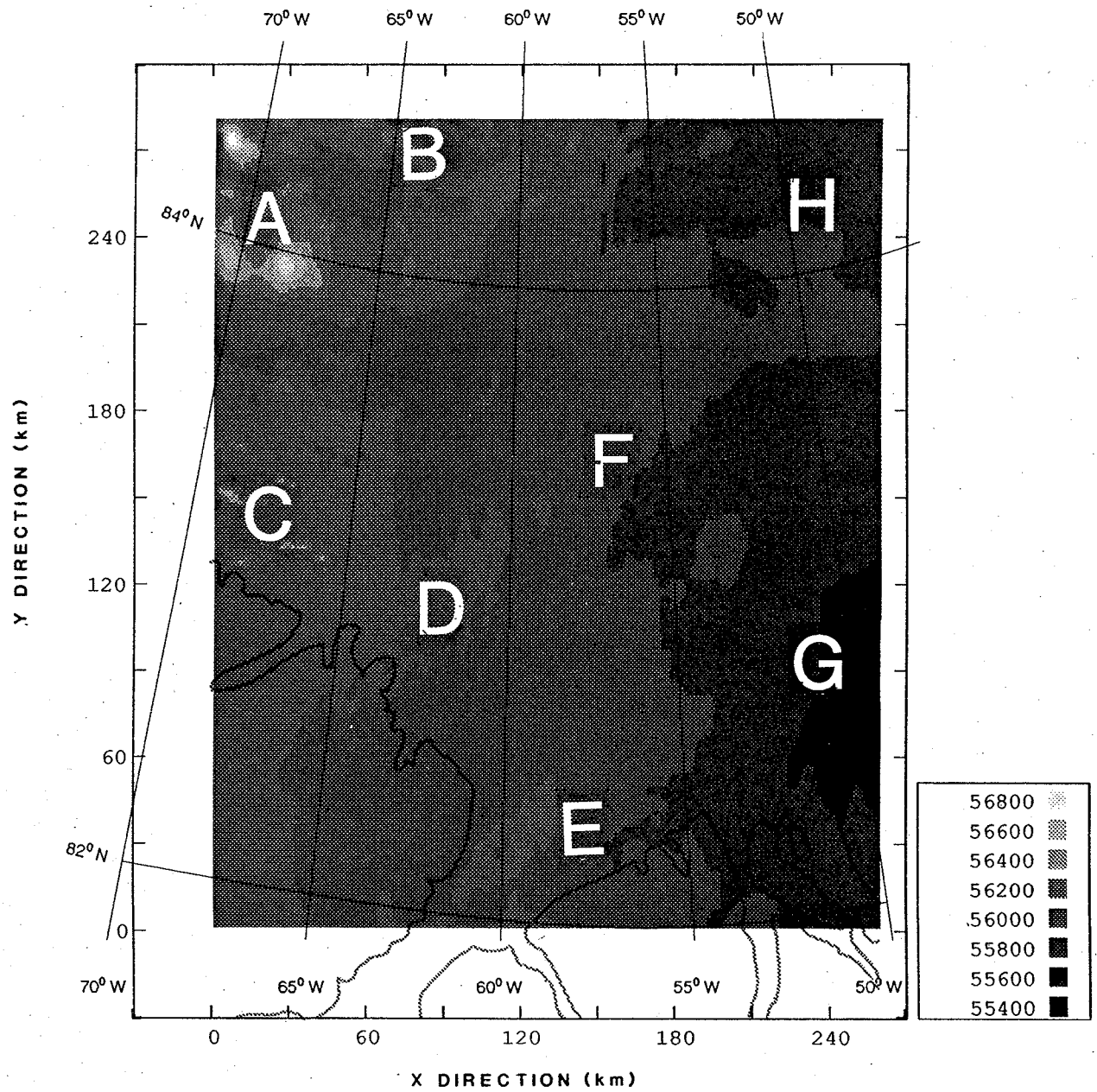
70° W
65° W
60° W
55° W
50° W
84° N
82° N
A
B
C
D
E
F
G
H
240
180
120
60
0
Y DIRECTION (km)
X DIRECTION (km)
56800
56600
56400
56200
56000
55800
55600
55400

Figure 8

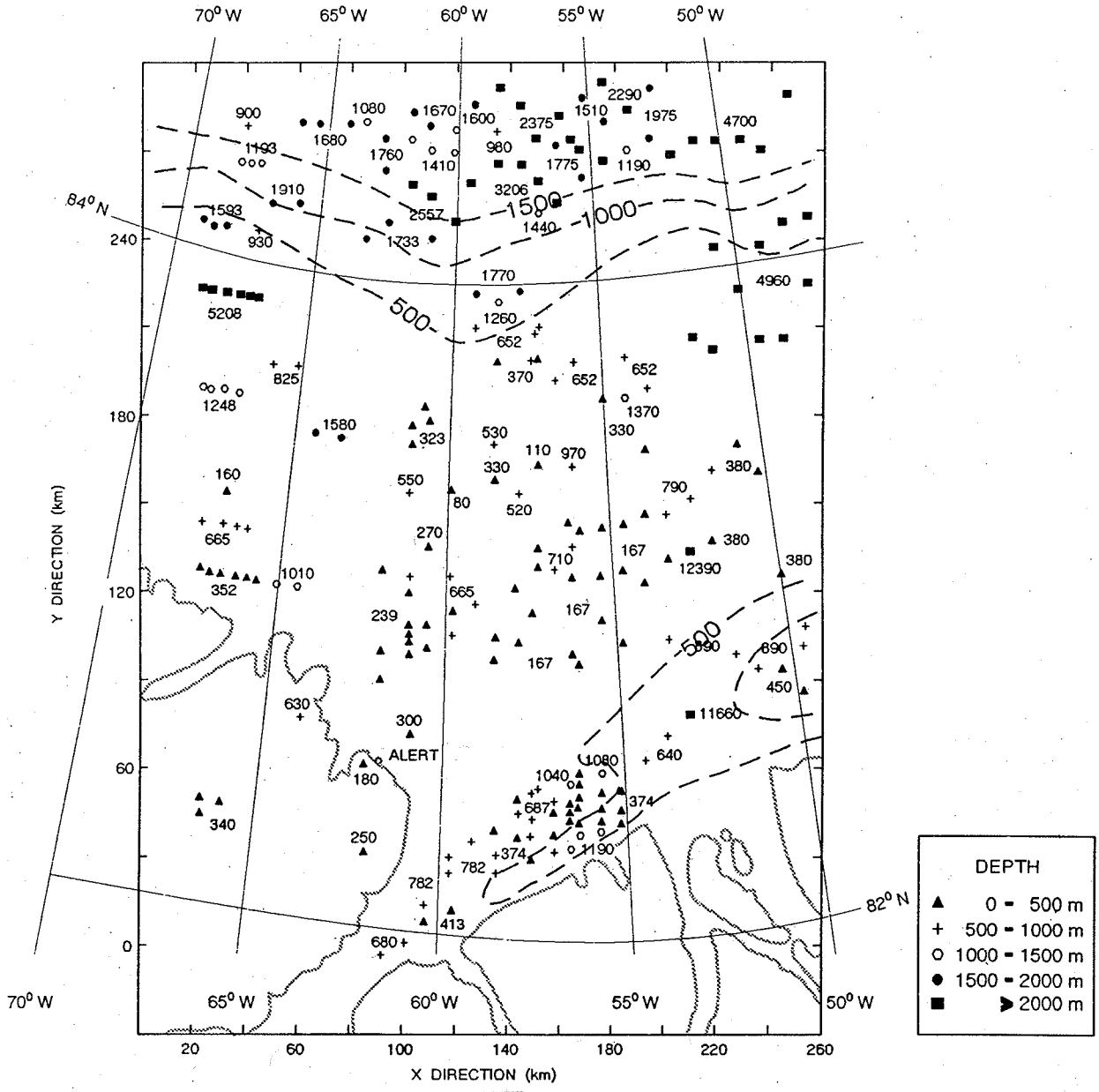
70° W
65° W
60° W
55° W
50° W
84° N
82° N
240
180
120
60
0
Y DIRECTION (km)
20
60
100
140
180
220
260
X DIRECTION (km)
ALERT
500
1000
1500
DEPTH
▲ 0 - 500 m
+ 500 - 1000 m
○ 1000 - 1500 m
● 1500 - 2000 m
■ > 2000 m

Figure 9